Supporting Information

Sustainable Development of Ultrathin Porous Carbon Nanosheet with Highly Accessible Defects from Biomass waste for High-Performance Capacitive Desalination

Silu Huo,[ab] Peng Zhang, [ab] Mingming He, [ab] Wei Zhang ,[ab] Bolong Liang,[c] Mingtao Zhang,[d] Hao Wang[ab], Kexun Li *[ab]*

a. The College of Environmental Science and Engineering, Nankai University, Tianjin 300071, China. E-mail: likx@nankai.edu.cn; Hao_WangNKU@163.com.
b. MOE Key Laboratory of Pollution Processes and Environmental Criteria, Tianjin Key Laboratory of Environmental Remediation and Pollution Control, Tianjin Key Laboratory of Environmental Technology for Complex Trans-Media Pollution, Nankai University, Tianjin 300071, China
c. College of Ecology and Environment, Hebei University, Baoding 071002, China
d. College of Chemistry, Nankai University, Tianjin 300071, P. R. China

S1. Materials and methods

1.1. Materials

Fresh lotus was purchase from Hubei province of China. Acetic acid, Potassium Chloride (KCl) and Lithium Chloride (LiCl) were purchased from Sinopharm Chemical Reagent Co. Ltd and used without further treatment. All the experiments in aqueous solution were carried out by using deionized (DI) water and all chemical reagents were of analytical grade.

1.2. Synthesis of C-A/S

The fresh lotus was broken into small pieces and freeze-dried. Next, 1.5 g dried lotus was dispersed into 10 wt % acetic acid aqueous solution and transferred into a Teflon-lined stainless-steel autoclave and heated at 120 °C for 4 h. After centrifugation and freezing drying, the product was fully mixed with 1.0 g LiCl and 4.0 g KCl. Further, the resulting mixture was carbonized under nitrogen atmosphere at 800 °C for 2 h. Finally, the C-A/S was obtained after the washing and drying process.

1.3. Synthesis of C-A

Similarly, C-A was obtained by the carbonization the acetic acid treatment product without the molten salt (LiCl and KCl) and the other steps remained the same.

1.4. Synthesis of C-S

Similarly, C-S was obtained by the carbonization the mixture of dried lotus and molten salt (LiCl and KCl) without the acetic acid treatment process and the other steps remained the same.

1.5. Synthesis of CB

CB sample was obtained by the direct carbonization dried lotus and the other steps remained the same.

S2. Characterization

2.1 Materials Characterization

The morphologies of samples were examined with field emission scanning electron microscopy (FE-SEM, Ultra Plus, Carl Zeiss, Germany) at an accelerating voltage of 5.0 kV. The carbons stick directly to the conductive adhesive. The structure of the samples was characterized by a transmission electron microscopy (TEM, JEM-2010 Japan). The carbons material is first ultrasonically dispersed in deionized water, then drops on the copper net. Raman spectra was recorded with a Raman spectrometer (Renishaw) with an argon ion laser (λ=514 nm). The Brunauer-Emmett-Teller (BET) surface area (SBET) of the powders was analyzed by nitrogen adsorption in a Micromeritics ASAP 2020 nitrogen adsorption apparatus (U.S.A.). All samples were degassed at 200 °C prior to nitrogen adsorption measurements. The specific surface areas were calculated using adsorption data by the multi-point Brunauer–Emmett–Teller (BET) method. Pore size distribution curves were computed using the nonlocal hybrid density functional theory (NLDFT) method assuming a slit/cylindrical pore geometry for the micropores and a cylindrical pore geometry for the mesopores. X-ray diffraction (XRD) of samples was performed on a diffractometer (D/Max-2400, Rigaku) advance instrument using Cu Kα radiation (k =1.5418 Å) at 40 kV, 100 mA. The 2θ range used in the measurements was from10 to 80°. X-ray photoelectron spectroscopy (XPS) measurement was performed on an Escalab 210 system (Germany) using a monochromatic Al Kα radiation source (ThermoVG Scientific). The AFM mode, Peak Force QNM, was used inorder to better control the force with which the tip interacts with thesurface. PPP-NCLR-20 probes with a force constant 21-98 N/m (silicon, resistivity: 0.01-0.02 Ωcm Bruker) were used for the ambient measurement.

2.2 Electrochemical measurements

Electrodes were prepared by mixing 80 wt. % of active material with 10 wt. % of

polytetrafluoroethylene (PTFE) binder (Aldrich, 60 wt. % suspension in water) and 10.0 wt. % carbon black in ethanol and then coated onto the graphite paper current collectors. The prefabricated electrodes dried at 80 °C for 12 h in a vacuum oven and were pressed under a pressure of 20 MPa for 3.0 min. The capacitive performance of electrode in three-electrode system was investigated in 1.0 M NaCl aqueous solution by a CHI760D electrochemical workstation (Chenhua Instruments Inc., Shanghai, China) with platinum wire and Hg/HgO electrode as counter and reference electrodes, respectively. Cyclic voltammetry (CV) test, galvanostatic charge-discharge (GCD) method and electrochemical impedance spectroscopy (EIS) analysis was conducted in the electrochemical studies. The specific capacitance derived from GCD was calculated by the equation: $Cg = \frac{I}{mdV/dt}$, where I is the constant current and m is the mass of active materials, as well as dV/dt is the slope obtained from fitting the discharge curve from the end of the voltage drop to the end of the discharge process. The specific capacitance derived from CV was calculated by the equation: $Cg = \frac{\int_{V1}^{V2} IdV}{2v\Delta Vm}$, where I is the response current (A), V_1 and V_2 represent the starting and ending potential, respectively, ΔV is the applied potential window (V), v is the potential scan rate (V/s), and m is the mass of active electrode material (g). The electrode size is 1 cm ×1 cm and the mass about 2.5 mg.

2.3 CDI characterization

For CDI characterization, we used the graphite paper as current collector, while the electrode materials were coated by a conventional blade coating method. For each electrode, the active material quality is 80 mg. The thickness of the electrode is approximately 0.4 mm and the single electrode area is 35 mm × 35 mm. The distance

between the electrodes is 2 mm. The volume of NaCl solution used is 160 mL. The peristaltic pumps drive the circulating flow of the NaCl solution at a flow rate of 10 mL min^{-1}. The conductivity meter is used to record the conductivity value of the NaCl solution flowing form the CDI device. The salt adsorption capacity (SAC, mg g^{-1}) was calculated according to the equation: $SAC = \frac{(c0 - c)Vs}{w}$, where C0 and C represent the initial and the final salt concentration (mg L^{-1}), and Vs is the volume of NaCl solution (L), as well as w is the total mass of active materials. Kim-Yoon plot was to evaluate the relationship between the salt adsorption capacity and the mean salt adsorption rate at the corresponding moment. The salt adsorption capacity (SACt, mg g^{-1}) and the salt adsorption rate (SAR, mg g^{-1} min^{-1}) at t minute were calculated by the following equations: $SACt = \frac{(C0 - Ct)Vs}{w}$ and $SAR = \frac{SACt}{t}$. The Ct is the concentration of NaCl solution at t minute and t (min) is the desalination process time. The discharging regeneration can be achieved through the short-circuited process and the operating time is about 65 mins. The charge efficiency of the electrode was obtained according to the following equation: $\varphi = \frac{SAC * F}{C}$, in which the SAC represents salt adsorption capacity (mg g^{-1}), F is the Faraday constant 96485 (C mol^{-1}) and C is calculated by integrating the charge current (C g^{-1}). For the cycling test, it is constantly cycling between short circuit and voltage application. The temperature during the whole capacitive deionization test is about 25 ℃. And the correlation between conductivity and salt concentration (NaCl) is 1 uS cm^{-1} = 0.505 mg L^{-1}.

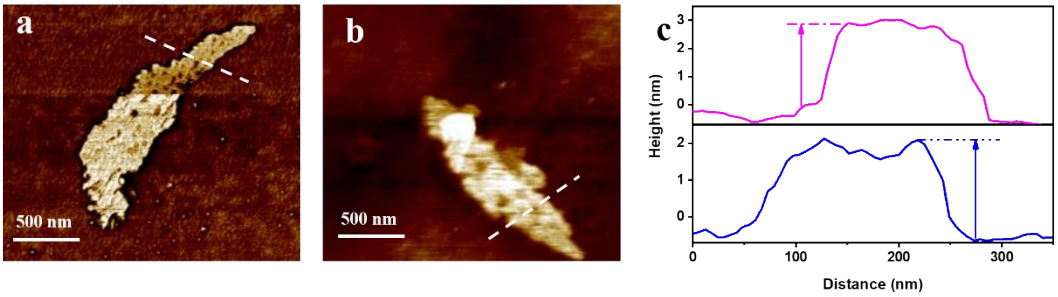

Figure S1.AFM images and corresponding height of C-A/S.

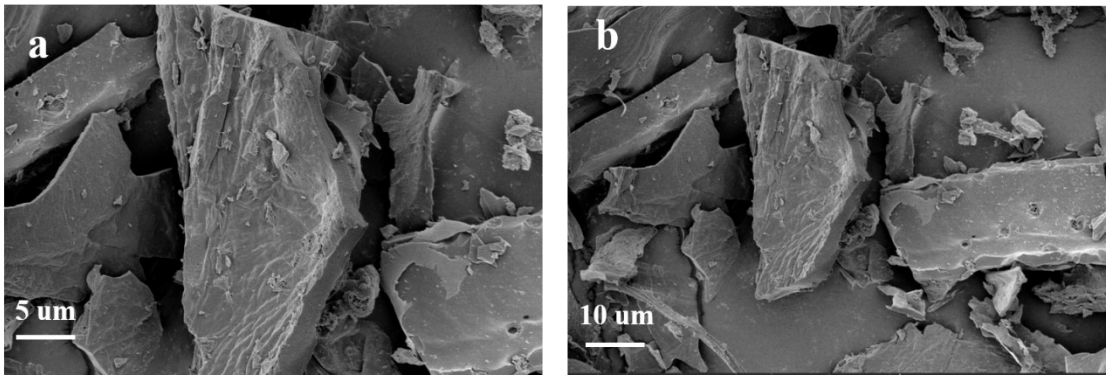

Figure S2. SEM images of CB.

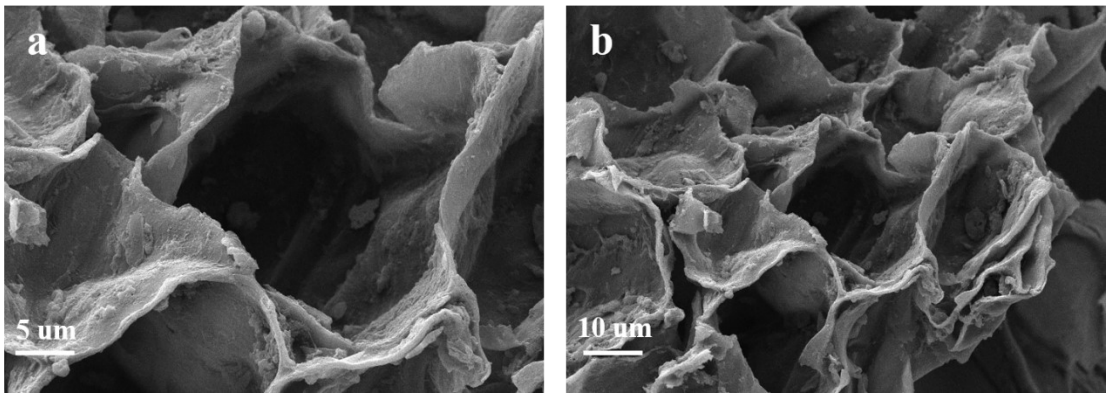

Figure S3. SEM images of C-A.

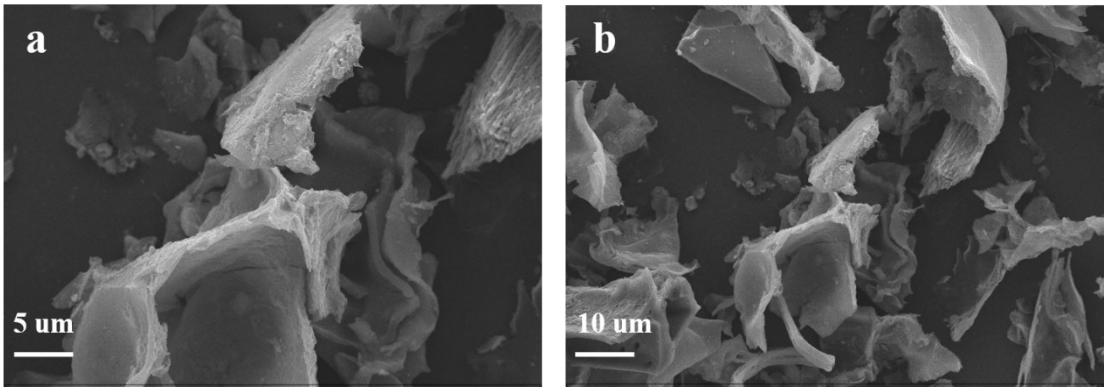

Figure S4. SEM images of C-S.

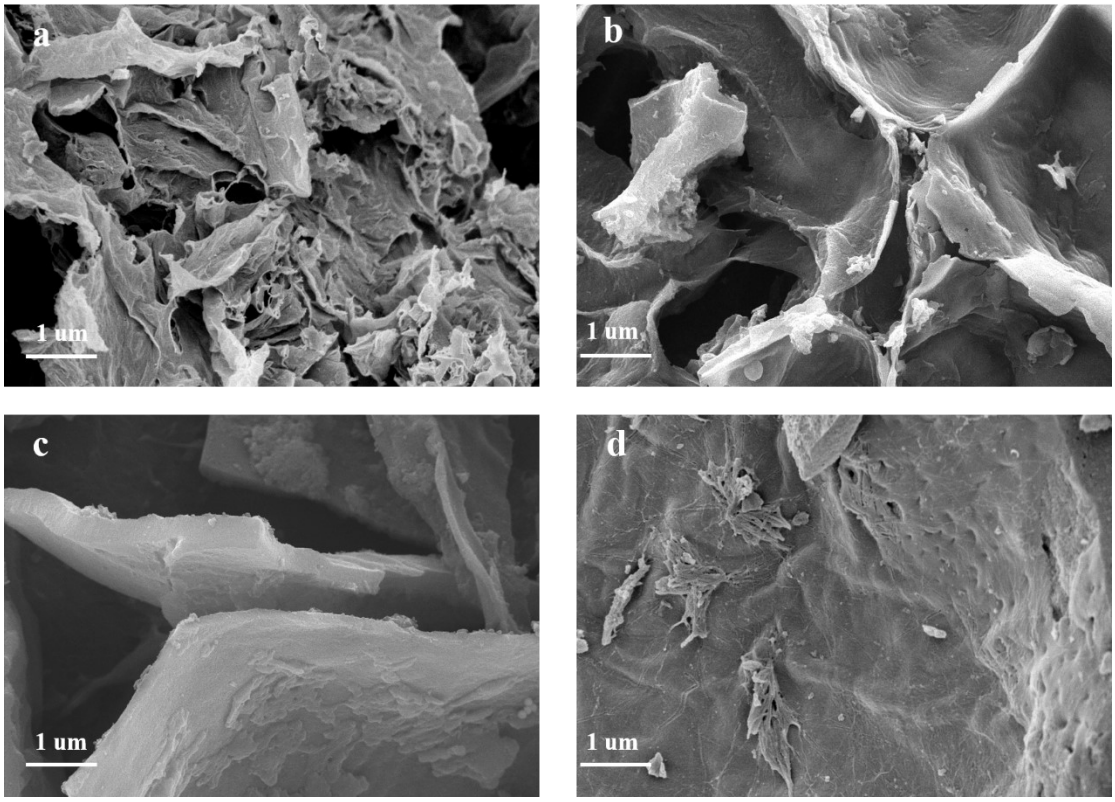

Figure S5. SEM images of SEM image of four samples at the same size. (a) C-A/S. (b) C-A. (c) C-S and (d) CB.

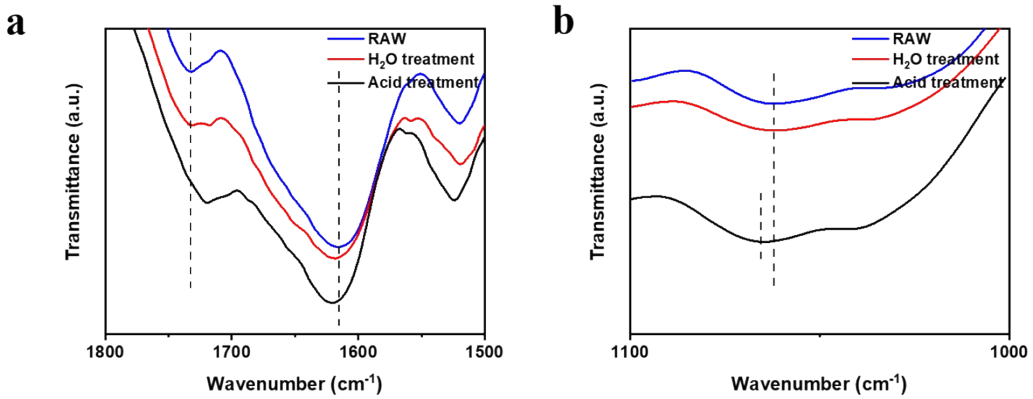

Figure S6. Partially enlarged FT-IR spectra of the raw material and precursors treated by H2O and acetic acid.

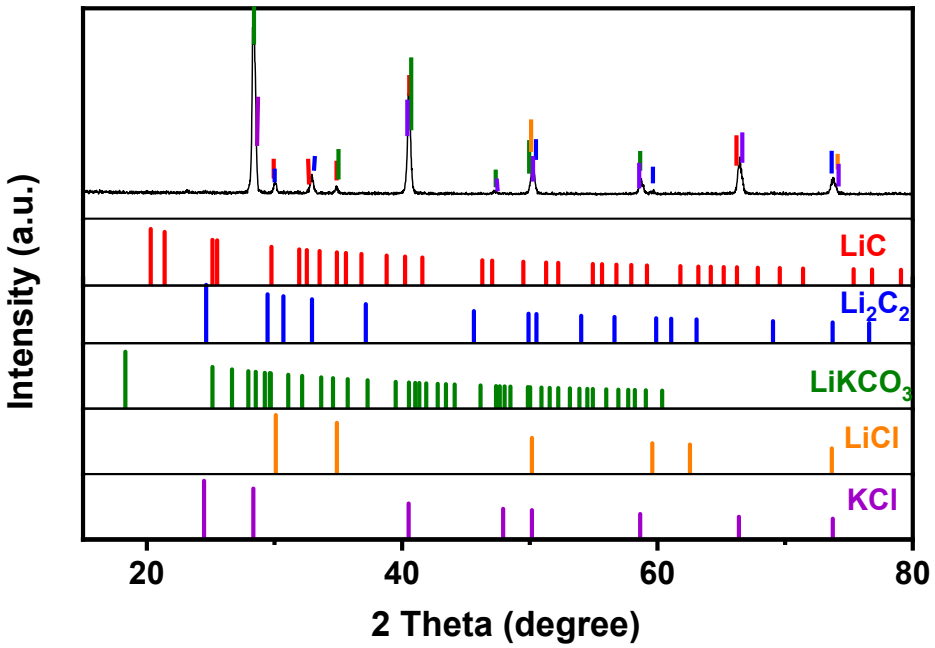

Figure S7. XRD patterns of produced metal impurities.

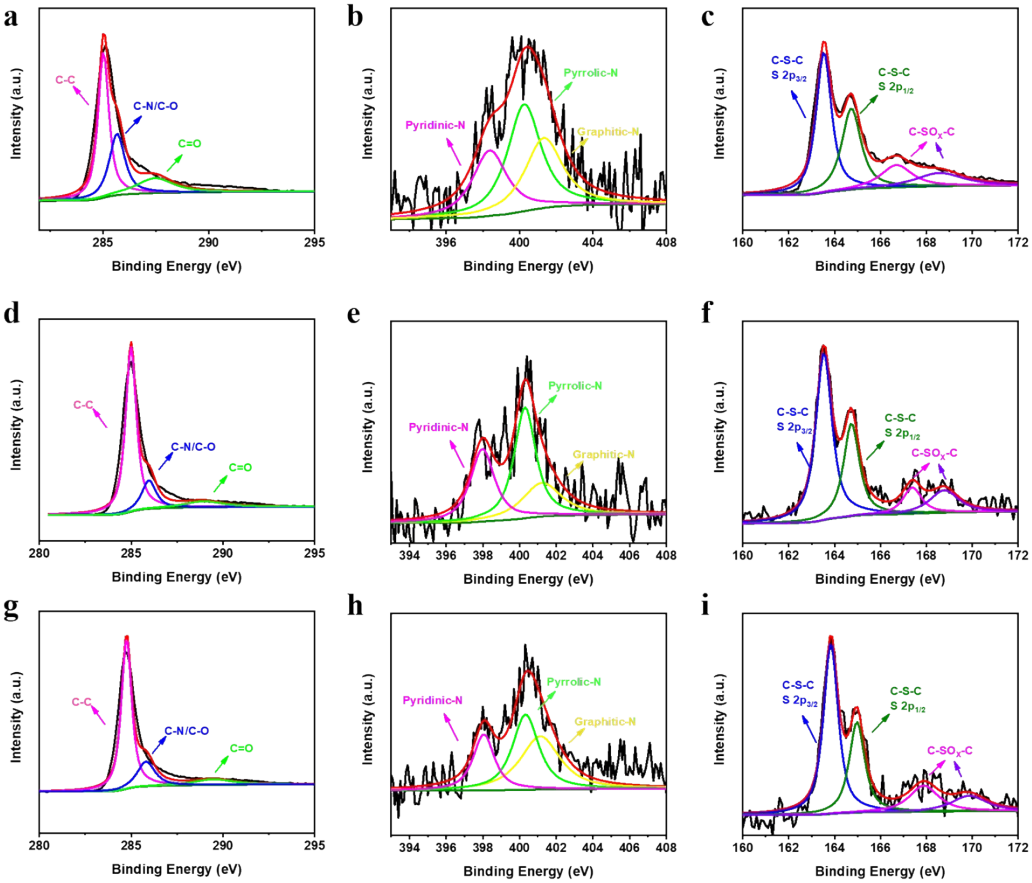

Figure S8. High-resolution C 1s, N 1s and S 2p spectra of (a-c) C-S. (d-f) C-A and (g-h) CB sample.

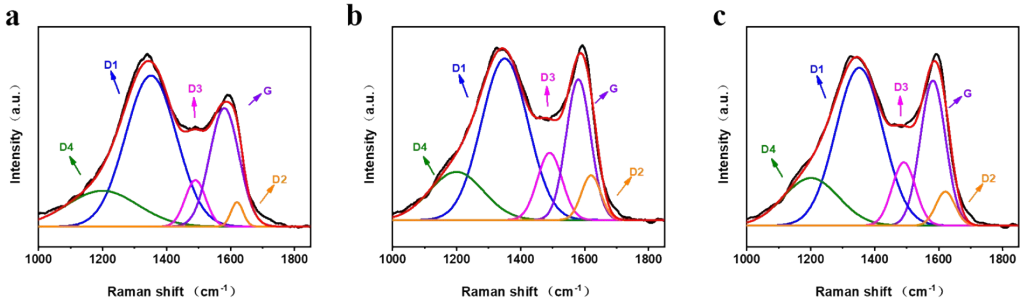

Figure S9. Raman spectra of (a) C-S. (b) C-A and (c) CB sample.

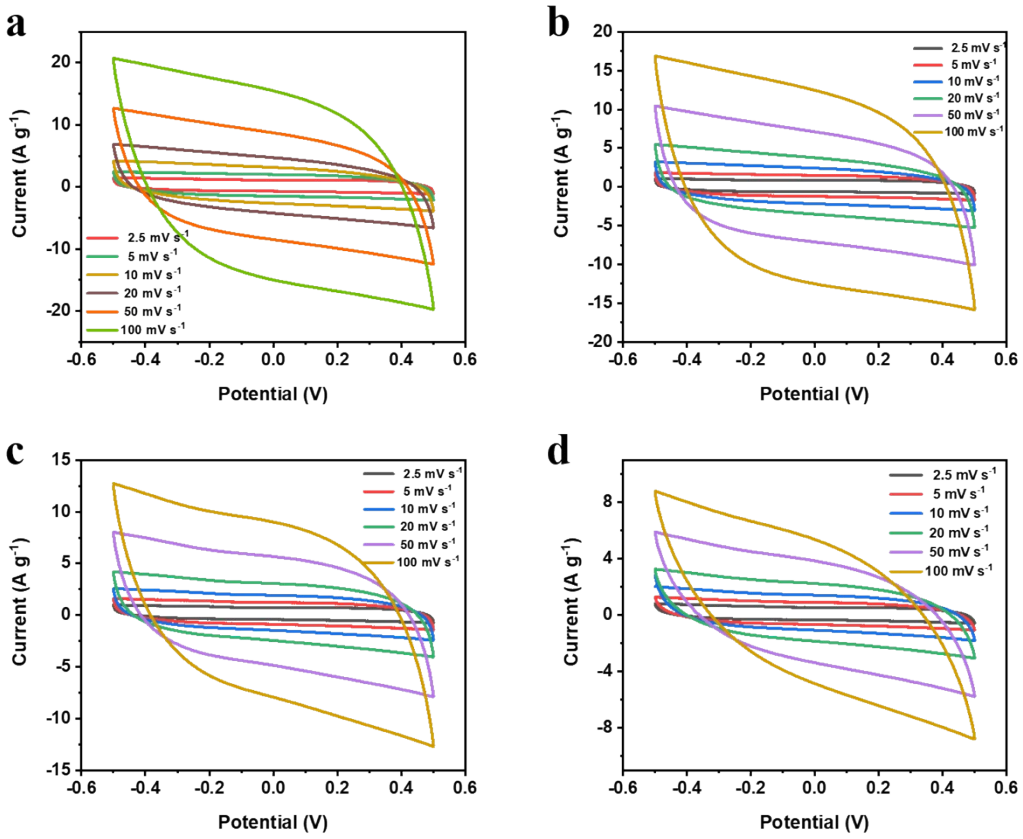

Figure S10. CV curves at different scan rates of (a) C-A/S. (b) C-S. (c) C-A and (d) CB.

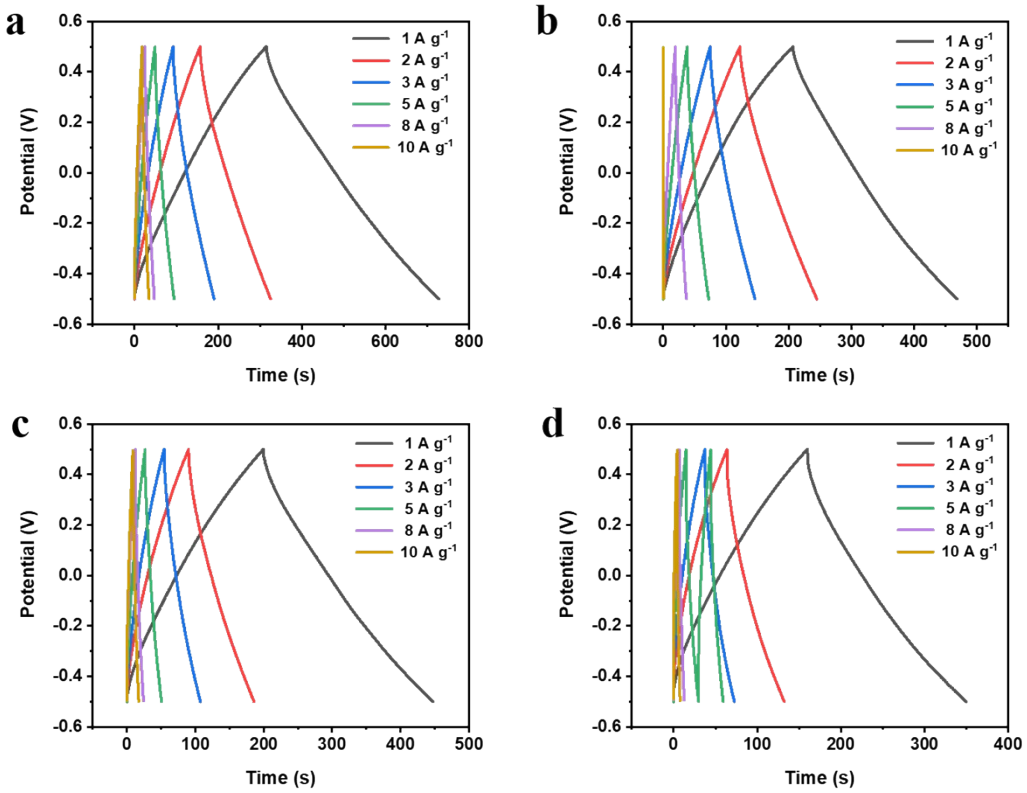

Figure S11. GCD curves at different current densities of (a) C-A/S. (b) C-S. (c) C-A and (d) CB.

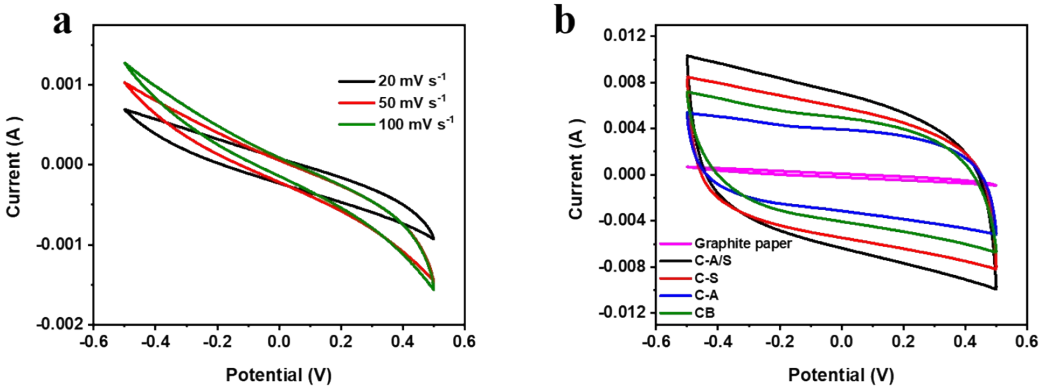

Figure S12. (a) CV curves at different scan rates of graphite paper. (b) CVs of different electrodes at a scan rate of 20 mV s^{-1}.

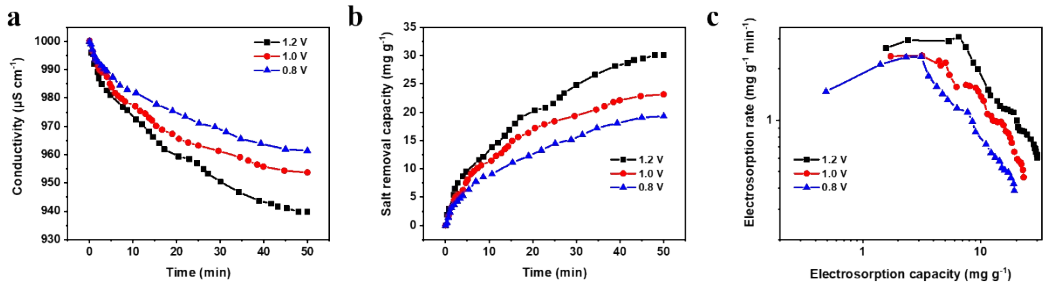

Figure S13. (a) Variation of solution conductivity vs. time. (b) SAC curves. (c) Kim-Yoon plots of C-A/S at different applied voltages.

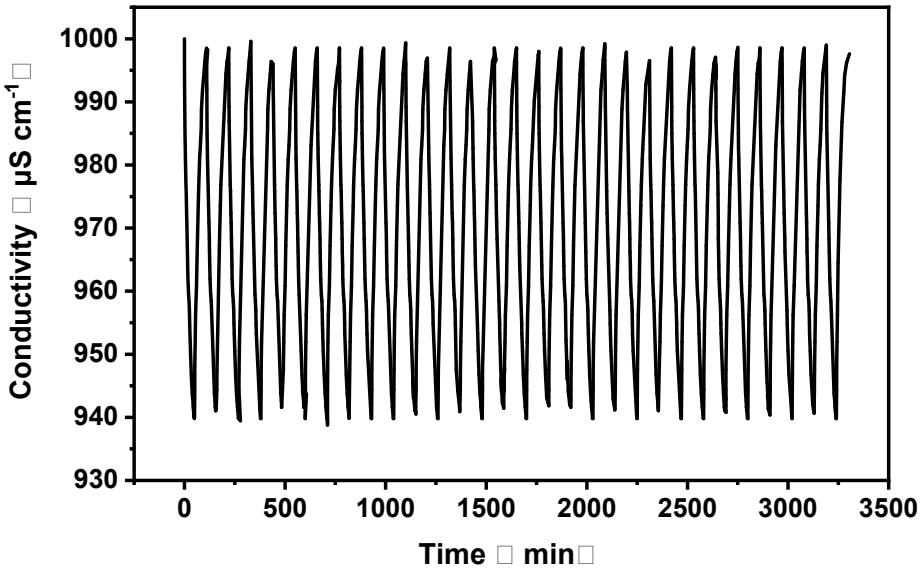

Figure S14. Regeneration stability of C-A/S.

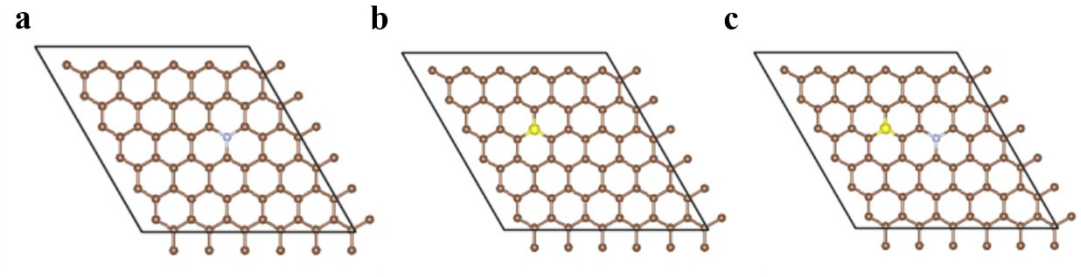

Figure S15. DFT models (a) N doped single layer graphene. (b) S doped single layer graphene. (c) N and S co-doped single layer graphene.

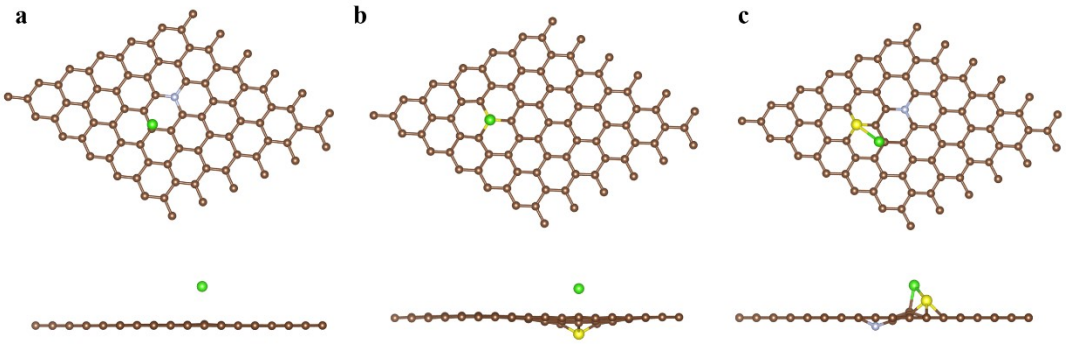

Figure S16. Top and side views of Cl adsorbed on (a) N-G, (b) S-G and (c) NS-G.

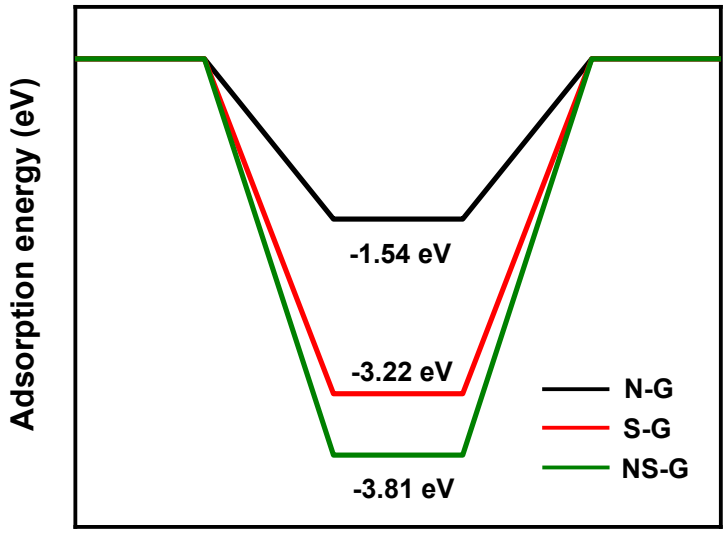

Figure S17. Adsorption energies of Cl on different samples.

Table S1 BET surface area and pore structure parameters of samples.

Samples	S_{BET} (m^2 g^{-1})	V_t (cm^3 g^{-1})	V_{micro} (cm^3 g^{-1})	V_{micro}/V_t
C-A/S	1586.7	1.07	0.70	65.4%
C-S	1398.1	0.75	0.57	76.0%
C-A	868.7	0.36	0.30	83.3%
CB	697.8	0.30	0.26	86.6%

Table S2 The Raman bands and vibration modes of graphite.

Band	Raman shift (cm^{-1})	Vibration mode
G	~1580	Ideal graphitic lattice
D1	~1350	Disordered graphitic lattice (graphene layer edges)
D2	~1620	Surface graphene layer
D3	~1490	Amorphous carbon
D4	~1200	Polyenes, ionic impurities

Table S3 Chemical compositions of as-prepared samples calculated from XPS results.

Samples	at.% C	at.% N	at.% O	at.% S
C-A/S	87.09	1.41	8.06	3.44
C-S	88.76	1.26	7.00	2.98
C-A	92.16	1.96	5.46	0.42
CB	93.52	1.17	4.98	0.33

Table S4. comparison of salt adsorption capacity with C-A/S and previous literatures.

Sample	Voltage (V)	Initial Concentration (mg/L)	Salt adsorption capacity (mg/g)	Ref.
e-CNF-PCP	1.2	500	12.56	1
NPC	1.2	500	21.4	2
3DGA-OP	1.2	500	14.4	3
hierarchical mesoporous carbon derived from ZIF-8	1.2	500	13.89	4
BCN nanosheets	1.4	500	13.6	5
ultrathin nitrogen-doped	1.2	500	17.52	6

carbon/graphene				
Carbon Nanocage	1.4	250	17.5	7
N-doped carbon sphere and holey graphene hydrogel	1.4	500	17.8	8
highly-ordered mesoporous carbon	1.2	500	14.6	9
B/N doped carbon nanosheets decorated with MnO_2	1.2	500	20.3	10
C-A/S	1.2	500	30.1	This work

[1] Y. Liu, J. Ma, T. Lu, L. Pan, *Sci. Rep.,* 2016, **6**, 32784.

[2] H. Wang, T. Yuan, L. Huang, W. Yang, *Sci. Total Environ.,* 2020, **720**, 137637.

[3] Y. S. Zhu, G. Zhang, *ACS Appl. Mater. Interfaces,* 2020, **12**, 29706-29716.

[4] T. Gao, Z. Liu, H. Li, *Sep. Purif. Technol.,* 2020, **231**, 115918.

[5] S. Wang, G. Wang, *J. Mater. Chem. A,* 2018, **6**, 14644-14650.

[6]M. Wang, X. Xu, J. Tang, L. Pan, Y. Yamauchi, *Chem. Commun.,* 2017, **53**, 10784.

[7] X. Zang, Y. Xue, W. Ni, C. Li, L. Hu, A. Zhang, Y. Yan, *ACS Appl. Mater. Interfaces,* 2020, **12**, 2180-2190.

[8] M. Mi, X. Liu, W. Kong, Y. Ge, W. Dang, J. Hu, *Desalination,* 2019, **464**, 18-24.

[9] X. Xu, H. Tan, L. Pan, T. Yang, Y. Yamauch, *Environ. Sci.: Nano,* 2019, **6**, 981.

[10] Z. Xie, X. Shang, J. Yang, B. Hu, J. Liu, *Carbon,* 2020, **158**, 184-192.

S3. Theoretical Calculations

The spin-polarized density functional theory (DFT) calculations were all performed by using the plane wave basis set based Vienna ab initio simulation package (VASP). Perdew-Burke-Ernzerhof (PBE) functional was adopted to describe the interaction between electrons and the cutoff energy of 450 eV was adopted for plane wave basis set. All the atoms were allowed to relax until the residue forces on each atom were less than 0.02 eV/Å. The graphene model used in our calculation consists of 12.30 × 29.83 × 15.00 $Å^3$. The vacuum region was set 20 Å in z direction to prevent the interaction between two adjacent surfaces. A 5×1×1 Monkhorst-Pack sampled k-points in the irreducible Brillouin zone for structure optimization. All the configurations are built by Material studio (MS).

To evaluate the stability of Na adsorbed on graphene nanoribbons, we calculated the adsorption energy (E_{ads}) of one Na on the surface as follows,

$$E_{ads} = E_{tot} - E_{surf} - E_{Na}$$

E_{tot} and E_{surf} are the total energies of graphene with and without Na adsorption, E_{Na} is the energy for single Na involved its bulk structures.